A tensor-based population value decomposition to explain rectal toxicity after prostate cancer radiotherapy.

Juan David Ospina, Frédéric Commandeur, Richard Ríos, Gaël Dréan, Juan Correa, Antoine Simon, Pascal Haigron, Renaud De Crevoisier, Oscar Acosta

A tensor-based population value decomposition to explain rectal toxicity after prostate cancer radiotherapy

Juan David Ospina [1 2 *] , Frédéric Commandeur [1] , Richard Ríos [1 2] , Gaël Dréan [1] , Juan Carlos Correa [2] , Antoine Simon [1] , Pascal Haigron [1] , Renaud De Crevoisier [1 3] , Oscar Acosta [1]

[1] LTSI, Laboratoire Traitement du Signal et de l'Image INSERM : U1099 , Université de Rennes 1 , Campus Universitaire de Beaulieu - Bât 22 - 35042 Rennes, FR

[2] Escuela de Estadística Universidad Nacional de Colombia (COLOMBIA) , Avenida Carrera 30 # 45, Bogotá, Cundinamarca 111321, CO

[3] Centre Eugène Marquis CRLCC Eugène Marquis , Avenue Bataille Flandres-Dunkerque 35042 Rennes Cedex, FR

* Correspondence should be addressed to: Juan David Ospina <jdospina@gmail.com >

Abstract

In prostate cancer radiotherapy the association between the dose distribution and the occurrence of undesirable side-effects is yet to be revealed. In this work a method to perform population analysis by comparing the dose distributions is proposed. The method is a tensor-based approach that generalises an existing method for 2D images and allows for the highlighting of over irradiated zones correlated with rectal bleeding after prostate cancer radiotherapy. Thus, the aim is to contribute to the elucidation of the dose patterns correlated with rectal toxicity. The method was applied to a cohort of 63 patients and it was able to build up a dose pattern characterizing the difference between patients presenting rectal bleeding after prostate cancer radiotherapy and those who did not.

Introduction

Radiotherapy is one of the prescribed treatments for prostate cancer. Its objective is to deliver high doses of radiation to the tumour cells whereas sparing the neighbouring organs, often called organs at risk (OAR). The prediction of normal tissue complication has traditionally being addressed using dose volume histograms (DVH) [1] or dose surface histograms (DSH) which are reductions of the 3D dose distribution received by the organs. Although many studies have shown a correlation between dose, volume and rectal toxicity [2,3], they lack spatial accuracy and are not able to correlate the treatment outcome with a specific dose pattern. One of the reasons is that normal tissue complication probability (NTCP) models mainly use the dosimetry information through the DVH, which does not preserve the spatial information. In radiotherapy is a well-known fact that similar DVHs may come from different dose distributions.

In the context of intensity modulate radiotherapy (IMRT) more adapted treatments could be proposed by including new constraints during the treatment planning step. Thus, the identification of anatomical regions correlated with toxicity is crucial to provide new recommendations for treatment planning. Some attempts have been made to introduce the notion of spatiality [4], but still within the dose-volume space. In [5] Buettner *et al.* have shown that late complications in the rectum are not only related to volumetric aspects of the dose, but particularly to the shape of the dose distribution. More recently, in [6,7] spatial considerations were incorporated by parametrizing the 3D patterns of dose. In this way, by selecting a limited set of predictive features, their method outperforms the classical models based on DVH/DSH. These approaches still lie in the reduction of feature dimensionality by fitting analytic functions to each dose shape. In [8] a principal components analysis (PCA) is developed. The PCA is applied on the registered dose matrices (expressed as row vectors) to obtain the principal modes of variation. Then, the modes of variation are used to classify patients according to a specific toxicity. The main issue of this work is the difficulty to interpret the results. Even if some principal components are related with a toxicity event, a spatial dose pattern is still hard to identify.

It would be desirable to have a method that allows for the identification of dose patterns. To accomplish this, we propose to generalise and use a population value decomposition (PVD) technique proposed in [9] for 2D image analysis. We propose a tensor-based generalisation of this PVD combined with a method to carry out statistical analysis that mimics the voxel-base morphometry (VBM) methods [10,11]. We show that the direct application of these methods, as proposed in [12], is difficult mainly because of the normality assumptions for the test statistics. In the end we show that it is possible to exhibit dose patterns associated with some type of toxicity following prostate cancer radiotherapy treatment.

Tensor-based population value decomposition

The tensor-based population value decomposition presented herein is a generalization of the PVD presented in [9]. In this former reference, a PVD method is developed using a possibly-truncated singular value decomposition (SVD) along with a PCA over the individuals' left- and right-singular eigen-vector matrices. This method enables compressing, thus leading to a more efficient representation of the subjects

Matrix-based population value decomposition

Consider a population consisting of *N* 2D images, $\mathbf{Y} \in \mathbb{R}$, *i* = 1, 2,…, *N*. The objective is to express **Y** as in eq. 1,

$$\mathbf{Y}_i = \mathbf{U}\mathbf{R}_i\mathbf{W},$$

(1)

where **U** and **W** are common to the whole population and **R** is specific to the *i*-th subject. The steps depicted in [9] to obtain the individuals' and the population matrices are as follows:

- Obtain the SVD of each image $\mathbf{Y}_i = \mathbf{S}_i\mathbf{V}_i\mathbf{D}_i^T$.

- Create the concatenated resulting matrices **S** = [**S** $_1$ /…/ **S**] and **D** = [**D** $_1$ /…/ **D**].

- Perform a PCA over **S** to obtain the eigen-vector matrix **U** of the covariance matrix **SS^T** such as **S** = **U** (**U S**).

- Perform a PCA over **D** to obtain the eigen-vector matrix **W** of the covariance matrix **DD^T** such as **D** = **W** (**W D**).

- Express **Y** in terms of the population matrices as

$$\mathbf{Y}_i = \mathbf{S}_i\mathbf{V}_i\mathbf{D}_i^T$$
$$= \mathbf{U}\{(\mathbf{U}^T\mathbf{S}_i)\mathbf{V}_i(\mathbf{D}_i^T\mathbf{W})\}\mathbf{W}^T$$

(2)

- Define $\mathbf{R}_i = (\mathbf{U}^T\mathbf{S}_i)\mathbf{V}_i(\mathbf{D}_i^T\mathbf{W})$ to obtain the decomposition **Y = UR W** .

The rationale behind this procedure is that the space spanned by the columns of **S** (or **D**) contains subject-specific left (or right) singular-vectors that, although they are not equal amongst them, they should be similar. Thus, applying PCA should allow for the calculation of the principal modes of variation of the left (or right) singular-vectors.

In addition, a more efficient representation could be obtained as a previous step to the population analysis. This decomposition allows for two different compression levels:

- At the individual's level some columns of **S** and **D** could be discarded regarding at some reconstruction error, leading to the approximation $\mathbf{Y}_i \approx \mathbf{S}_{L_i}\mathbf{V}_{L_iJ_i}\mathbf{D}_{J_i}^T$, where **S** $_{L_i}$ is the matrix resulting of taking only the first *L* columns of **S** , **D** $_{J_i}$ is the analogous with respect to **D** and **V** $_{L_iJ_i}$ consists only of the first *L* columns and the first *J* rows of **V** .

- At the population level it is possible to take only the first *A* columns of **U** (or the first *B* columns of **W**), considering for example the explained percentage of variance, to build up the projection matrix **U** (or **W**). The same reduction is possible when the PCA is performed over **S** = [**S** $_{L_1}$|…|**S** $_{L_N}$] and **D** = [**D** $_{J_1}$|…|**D** $_{J_N}$], with $L = \Sigma_{i=1}^{N}L_i$ and $J = \Sigma_{i=1}^{N}J_i$.

As one can notice, the resulting individual specific matrices **R** are not diagonal. This matrices can be regarded as projections onto a subspace of $\mathbb{R}$, with $A \leq F$ and $B \leq G$.

Extension to 3D images

In the following approach the fact that a 3D image can be regarded as a third-order tensor is used. The SVD step of the 2D-PVD described before is emulated using a higher order singular value decomposition (HOSVD) [13]. The population consists of 3D images, $\underline{\mathbf{Y}} \in \mathbb{R}$, *i* = 1, 2, …, *N*, regarded as tensors.

The procedure to obtain a 3D-PVD was implemented as follows:

- Obtain the HOSVD of each image as in eq. (3),

$$\underline{\mathbf{Y}}_i = \mathbf{V}_i \times_1 \mathbf{S}_i^1 \times_2 \mathbf{S}_i^2 \times_3 \cdots \times_M \mathbf{S}_i^M, i = 1, \ldots, N,$$

(3)

where $\underline{\mathbf{V}}$ is the core tensor and $\mathbf{S}_i^1, \ldots, \mathbf{S}_i^M$ are the corresponding factor matrices. For a 3D image *M* = 3.

- Create the *M* matrices $\mathbf{S}^k = [\mathbf{S}_1^k | \cdots | \mathbf{S}_N^k]$, *k* = 1, …, *M*.

- Perform a PCA over each **S** to obtain the projection matrices **P** such as **S** = **P** (**P**) **S** , *k* = 1, …, *M*.

- Express each individual's image as in eq. (4),

$$\underline{\mathbf{Y}}_i = \Lambda_i \times_1 \mathbf{P}^1 \times_2 \cdots \times_M \mathbf{P}^M,$$

(4)

where $\Lambda_i = \mathbf{V}_i \times_1 (\mathbf{P}^1)^T \mathbf{S}_i^1 \times_2 \cdots \times_M (\mathbf{P}^M)^T \mathbf{S}_i^M$.

As it can be seen from eq. (4), the image corresponding to the *i*-th individual can be expressed in terms of a specific-individual core tensor, namely Λ_i, and *M* population factor matrices. In addition, as in the 2D case, two compression levels are allowed:

- At the individual's level each image can be expressed as in eq. (5),

$$\underline{\mathbf{Y}}_i \approx \hat{\mathbf{V}}_i \times_1 \mathbf{S}_{L_i^1}^1 \times_2 \mathbf{S}_{L_i^2}^2 \times_3 \cdots \times_M \mathbf{S}_{L_i^M}^M,$$

(5)

where $\mathbf{S}_{L_i^k}^k$ is a matrix consisting of the the first L_i^k columns of $\mathbf{S}_i^k$, and $\hat{\mathbf{V}}_i \in \mathbb{R}^{L_i^1 \times \cdots \times L_i^M}$ is the truncated core tensor.

- At the population level the **P** matrices can be truncated by taking only the first Q columns leading to the reduced matrix $\mathbf{P}^{Q_k}$. The same reduction is possible when the PCA is carried out on $\mathbf{s}^{L^k} = [\mathbf{s}_{L_1^k}^k \mid \cdots \mid \mathbf{s}_{L_N^k}^k]$.

Using both levels of compression the *i*-th invididual's image can be approximated as in eq (6),

$$\underline{\mathbf{Y}}_i \approx \Lambda_i \times_1 \mathbf{P}^{Q_1} \times_2 \cdots \times_M \mathbf{P}^{Q_M},$$

(6)

where $\Lambda_i = \hat{\mathbf{V}}_i \times_1 (\mathbf{P}^{Q_1})^T \mathbf{S}_{L_i^1}^1 \times_2 \cdots \times_M (\mathbf{P}^{Q_M})^T \mathbf{S}_{L_i^M}^M$ is the *i*-th individual's core tensor and $\mathbf{P}^{Q_1}$, ..., $\mathbf{P}^{Q_M}$ are the population factor matrices.

Population analysis

Once each individual has been rewritten as in eq. (6) the statistical analyses can be carried out using the reduced individuals' representation Λ_i, *i* = 1, ..., *N*. If the population can be split into two mutually exclusive groups, say G_1 and G_2, an element-by-element comparison of the elements of Λ could help to highlight the differences amongst both groups. This comparison can be done using a two-sample t-test. The resulting p-values could be used then to decide which components are different amongst the two groups. Let $\Lambda^{(G_1)}$ and $\Lambda^{(G_2)}$ be the typical core tensors of groups G_1 and G_2, respectively, with components $\lambda_{mnp}^{(G_1)}$ and $\lambda_{mnp}^{(G_2)}$. In addition, let $\underline{\mathbf{Pv}}$ be the resulting p-value tensor with entries *pv*. In this work the components of $\Lambda^{(G_1)}$ and $\Lambda^{(G_2)}$ are calculated as $\lambda_{mnp}^{(G_j)} = \frac{1}{|G_j|} \sum_{i \in G_j} \lambda_{mnp}$, *j* = 1, 2 if $pv < p$ and $\lambda_{mnp}^{(G_j)} = \frac{1}{|G_1 \cup G_2|} \sum_{i \in G_1 \cup G_2} \lambda_{mnp}$ otherwise, where *p* is some specified threshold. It means that for the components where no statistical difference is found the reconstruction is done using the information of the whole population whereas for those components where a statical difference is accepted the component reconstruction is done with the information coming from either one group or the other.

Using this approach the typical images for each group can be reconstructed as shown in eq. (7),

$$\underline{\mathbf{Y}}^{(G_j)} = \Lambda^{(G_j)} \times_1 \mathbf{P}^{Q_1} \times_2 \cdots \times_M \mathbf{P}^{Q_M}, \; j = 1, 2.$$

(7)

Rectal bleeding study

Data

A total of 63 patients treated for localized prostate cancer with IMRT were included in the study. The used treatment planning system was Pinnacle V7.4 (Philips Medical System, Madison, WI). The total prescribed dose was 46 Gy to the seminal vesicles delivered in 4.6 weeks, and 80 Gy to the prostate delivered in 8 weeks, with a standard fractionation of 2 Gy/fraction. The patient positioning, CT acquisition, volume delineations and dose constraints complied with the GETUG 06 recommendations as described in [14]. For the rectal wall, the constraints were maximal dose ≤76 Gy and V72 Gy≤25% (the volume received by the 72% of the rectum wall volume). The CT images consisted of 135 slices whose size in the axial plane was 512×512 pixels, with 1mm image resolution and 2mm slice thickness. The median follow-up period was 38 months, with a minimum of 24 months for all patients. Rectal toxicity events were prospectively collected and scored according to the common terminology criteria for adverse events (CTCAE) version 3.0. The endpoint of the study was 2-year Grade ≥1 rectal bleeding, excluding acute toxicity. Patients with a history of hemorrhoids were not allowed to be scored as Grade 1 bleeding. In total, 12 patients presented at least a Grade 1 rectal bleeding event, which occurred between 6 and 24 months following the treatment.

Image processing

Patient's planned CT and dose distributions were non-rigidly registered with the demons algorithm [15], on a single coordinate system by combining the CTs and organs delineations as explained in [8]. The patients' CTs were first registered and then the same transformation was applied to the dose distributions in order to obtain the mapped dose distributions to a single template that were compared in this work.

The dose images were cropped in the axial plane to be of size 87 × 87 and only 51 slices were considered. Each dose was decomposed using the HOSVD as shown in eq. (3) and no compression was allowed for at the individual or population levels as the interest was the precise identification of dose patterns.

Once all the patients' core tensors were computed, an element-wise comparison was performed in the core tensor space using a two-sample t-test, considering the patients who presented at least a Grade 1 rectal bleeding event against to those who did not. A p-value lower than 0.05 was considered statistically significant. A "typical" core tensor for each group was calculated. Each element of the typical core tensors was computed as an average of the corresponding element across the population. For those elements that were found to be statistically different the average was computed using only the values of the corresponding group. For the remaining elements the average was computed using both groups values. The "typical" dose image for each group was reconstructed using the corresponding "typical" core tensor and the population factor matrices. The difference amongst the two "typical" dose distributions was used to find regions correlated with rectal bleeding Grade ≥ 1.

Results

The Fig. 1(a) shows the difference between the "typical" bleeder individual and the "typical" non-bleeder individual obtained with the proposed method. This result suggest an over irradiation (around 6 Gy) on patients presenting rectal bleeding Grade ≥ 1 in the zone of the posterior wall. For the sake of comparison in Fig. 1(b), the difference of the means of the bleeders' doses and the non-bleeders' doses is presented. The normality assumption was checked using a Shapiro-Wilk test in the core tensor space with a 95% confidence level. Only on the 22% of the elements the normal assumption was rejected. This test was also performed in the native image space and the normality assumption was rejected on the 67% of the voxels. Conversely, in the tensor case, no difference was detected on the elements where the normality assumption was rejected. To illustrate the problem of normality assumptions, and then the validity of performing a two-sample t-test in the native space, Fig. 2 shows the histograms of the test statistics for both cases: the tensor case and the native image space. It is expected, if the normality assumption is valid, that the normalized histograms look like a standard normal distribution. This is the case for the tensor-based test statistics but not for those computed in the native image space.

Conclusions

This paper presented a method to perform population analysis for high order data ($M > 2$) and its application to the study of rectal bleeding after prostate cancer radiotherapy. The presented method does not depend on the type of toxicity and it could be applied to find out other dose patterns correlated with different side effects, even in a different organ (such as the bladder). The main contribution of the tensor-based PVD was to enable the use of a classical statistic test to perform group comparison through the construction of the "typical" individual for both groups. The obtained results should be carefully interpreted as the over irradiated zone depicted in Fig. 1(a) could depend on the selected template for registering all the images but also on the registration algorithm. Future work will include the segmentation of this zone and the study of the associated DVHs.

The direct application of the t-test over the dose images is not advised as normality assumption is rejected for most of the voxels. This is not the case in the core tensor space, however, highlighting the zones where both group are statistically different in the native image space is a subject of current research.

A future works will include as well a tensor-based PVD of each group and attempting to reveal the inter-group differences by the comparison of the population matrices. The effect of applying some level of compression at the individual's or population level and the validity of the method are also matter of future studies.

References:

- 1 . Ting JY , Wu X , Fiedler JA , Yang C , Watzich ML , Markoe A . Dose-volume histograms for bladder and rectum . Int J Radiat Oncol Biol Phys . 38 : 1997 ; 1105 - 1111
- 2 . Sohn M , Alber M , Yan D . Principal component analysis-based pattern analysis of dose-volume histograms and influence on rectal toxicity . Int J Radiat Oncol Biol Phys . 69 : 2007 ; 230 - 239
- 3 . Fiorino C , Vavassori V , Sanguineti G , Bianchi C , Cattaneo GM , Piazzolla A , Cozzarini C . Rectum contouring variability in patients treated for prostate cancer: impact on rectum dose-volume histograms and normal tissue complication probability . Radiother Oncol . 63 : 2002 ; 249 - 255
- 4 . Kupchak C , Battista J , Dyk JV . Experience-driven dose-volume histogram maps of NTCP risk as an aid for radiation treatment plan selection and optimization . Med Phys . 35 : 2008 ; 333 - 343
- 5 . Buettner F , Gulliford SL , Webb S , Sydes MR , Dearnaley DP , Partridge M . Assessing correlations between the spatial distribution of the dose to the rectal wall and late rectal toxicity after prostate radiotherapy: an analysis of data from the mrc rt01 trial (isrctn 47772397) . Physics in Medicine and Biology . 54 : 2009 ; 6535 -
- 6 . Buettner F , Gulliford SL , Webb S , Partridge M . Modeling late rectal toxicities based on a parameterized representation of the 3d dose distribution . Physics in Medicine and Biology . 56 : 2011 ; 2103 -
- 7 . Lee R , Chan EK , Kosztyla R , Liu M , Moiseenko V . Dose-distance metric that predicts late rectal bleeding in patients receiving radical prostate external-beam radiotherapy . Physics in medicine and biology . 57 : 2012 ; 8297 -
- 8 . Chen B , Acosta O , Kachenoura A , Ospina J , Dréan G , Simon A , Bellanger JJ , Haigron P , Crevoisier R . Spatial characterization and classification of rectal bleeding in prostate cancer radiotherapy with a voxel-based principal components analysis model for 3d dose distribution . Editor: Madabhushi A , Dowling J , Huisman H , Barratt D . Prostate Cancer Imaging. Image Analysis and Image-Guided Interventions. Volume 6963 of Lecture Notes in Computer Science . Springer ; Berlin Heidelberg 2011 ; 60 - 69
- 9 . Crainiceanu CM , Caffo BS , Luo S , Zipunnikov VM , Punjabi NM . Population value decomposition, a framework for the analysis of image populations . Journal of the American Statistical Association . 106 : 2011 ; 775 - 790

- 10 . Friston K , Holmes A , Worsley K , Poline J , Frith C , Frackowiak R . Statistical parametric maps in functional imaging: a general linear approach . Human brain mapping . 2 : 1994 ; 189 - 210
- 11 . Ashburner J , Friston K . Nonlinear spatial normalizatioon using bbasis functions . Human Brain Mapping . 7 : 1999 ; 254 - 266
- 12 . Acosta O , Drean G , Ospina JD , Simon A , Haigron P , Lafond C , De Crevoisier R . Voxel-based population analysis for correlating local dose and rectal toxicity in prostate cancer radiotherapy . Physics in medicine and biology . 58 : 2013 ; 2581 -
- 13 . De Lathauwer L , De Moor B , Vandewalle J . A multilinear singular value decomposition . SIAM J Matrix Anal Appl . 21 : 2000 ; 1253 - 1278
- 14 . Beckendorf V , Guerif S , Le Prisé E , Cosset JM , Bougnoux A , Chauvet B , Salem N , Chapet O , Bourdain S , Bachaud JM , Maingon P , Hannoun-Levi JM , Malissard L , Simon JM , Pommier P , Hay M , Dubray B , Lagrange JL , Luporsi E , Bey P . 70 gy versus 80 gy in localized prostate cancer: 5-year results of getug 06 randomized trial . International Journal of Radiation Oncology*Biology*Physics . 80 : 2011 ; 1056 - 1063
- 15 . Thirion JP . Image matching as a diffusion process: an analogy with maxwell's demons . Medical image analysis . 2 : 1998 ; 243 - 260

Figure 1

"Typical" toxic dose distribution minus "typical" non-toxic dose distribution. The rectum of the template patient in the sagital plane is overlaid.

(a) Tensor-based PVD difference of means.

(b) Simple difference of means.
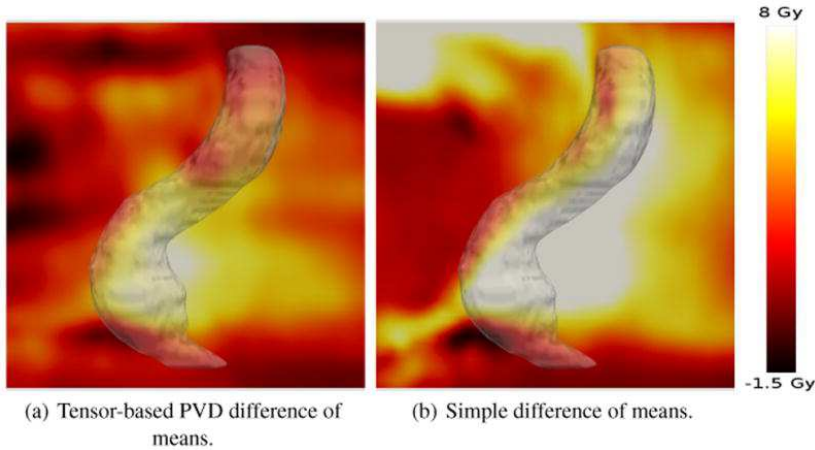
Figure 2

Histograms of the test statistics used in the t-test.

(a) Tensor-based test statistic histogram.

(b) Native space test statistic histogram.